Int. J. Electrochem. Sci., 14 **(2019)** 2422 – 2429, doi: 10.20964/2019.03.82

International Journal of
ELECTROCHEMICAL
SCIENCE
www.electrochemsci.org

Synthesis and Electrochemical Characterization of α-$NaMnO_2$ as a Cathode Material for Hybrid Na/Li-Ion Batteries

*Liming Zhang[1,2], Yanhui Zhang[1,2], Zhi Su[*1,2], Hualing Tian[1,2], Lei Wang[1]*

[1] College of Chemistry and Chemical Engineering, Xinjiang Normal University, Urumqi, 830054, Xinjiang, China
[2] Engineering Research Center Of Electrochemical Technology and Application, Xinjiang Normal University, Urumqi, 830054, Xinjiang, China
[*]E-mail: suzhixj@sina.com

Received: 11 November 2018 / *Accepted:* 2 January 2019 / *Published:* 7 February 2019

The monoclinic α-$NaMnO_2$ can be successfully prepared by a simple high-temperature solid-phase method . Herein, we use instrumental techniques to characterize and investigate its performance as a cathode material for hybrid Na/Li-ion batteries, demonstrating that the obtained product comprises ~100-nm-sized particles and is a mixture of α-$NaMnO_2$ and P2-$Na_{0.7}MnO_2$. Electrochemical performance testing reveals the presence of well-pronounced charge and discharge plateaus in charge/discharge curves and shows that the highest initial discharge capacity of 195.6 mAh/g (at 2–4 V and 12.2 mAh/g) is observed for α-$NaMnO_2$ prepared by 12-h sintering at 800 °C and decreases to 100.9 mAh/g after 30 cycles.

Keywords: α-$NaMnO_2$, high-temperature solid-phase synthesis, mixed crystal, hybrid battery, energy storage

1. INTRODUCTION

Currently, mankind is faced with several environmental and energy problems of global importance, such as the overexploitation-induced depletion of fossil fuel reserves and the related issues of global warming and haze, which necessitates the search for recyclable green energy sources and large-scale energy storage systems [1]. To date, large-scale energy storage is commonly accomplished using lithium-ion batteries, which feature the advantages of high energy density, long lifetime, and insignificant environmental footprint [2,3]. However, the widespread use of these batteries is hindered by the scarcity and high cost of lithium resources [4]. Compared to lithium, sodium is much cheaper and more naturally abundant, and sodium-ion batteries (NIBs) are therefore viewed as a promising alternative to lithium-ion batteries [5–7]. At present, several compounds have been explored as NIB

cathode materials, e.g., transition metal (Me) oxides [8,9], phosphates [10,11], and fluorophosphates [12,13]. Among these materials, $NaMeO_2$ species are considered to be most promising in view of their ease of synthesis and high theoretical capacity, and have therefore been extensively studied [14]. In particular, $NaCrO_2$ [15], Na_xCoO_2 [16], and Na_xMnO_2 [17–19] feature high discharge capacities of 100–150 mAh g^{-1} at 2–4 V vs. Na/Na^+. Although NIBs have many advantages, the higher molecular weight of Na compared to that of Li results in reduced energy density of NIB materials. In addition, Na^+ has a larger radius than Li^+, which may impede the insertion/deintercalation of the former into/from the host material lattice and necessitates the use of structural modifications to realize high electrochemical performance [20]. Among the large number of potential NIB battery materials, those based on Mn oxides (e.g., Na_xMnO_2) have attracted much attention in view of their low cost and environmentally friendly nature [18]. However, these materials suffer from sodium ion insertion/deinsertion–induced structural degradation and capacity decay, and are typically converted into an amorphous phase after only eight electrochemical cycles, which can be ascribed to the Jahn-Teller effect of the Mn^{3+}/Mn^{4+} redox reaction [21]. Consequently, various attempts have been made to improve the cycling stability of Na_xMnO_2, e.g., by controlling morphology and particle size [22,23] via the choice of proper high-temperature solid-phase [24], hydrothermal [25,26], and sol-gel [27] methods.

Delmas et al. [28] proposed that layered Na_xMeO_2 compounds are of the O3 or P2 type and feature sodium ions arranged at octahedral and prismatic sites sandwiched between MeO_2 slabs, respectively. Caballero et al. [21] demonstrated that although $Na_{0.6}MnO_2$ prepared by a sol-gel method displays an initial discharge capacity of 140 Ah/kg at a current density of 0.1 mA/cm^2 and voltages of 2–3.8 V (vs. Na/Na^+), the continuous insertion and extraction of Na^+ induce a progressive collapse of the host structure to yield an amorphous material, resulting in a gradual reduction of cell capacity. Ruffo et al. [18] described a modified Pechini method–based synthesis of $Na_{0.44}MnO_2$, demonstrating that this material exhibits a good initial discharge capacity (~110 mAh/g) at a low current rate (11 mA/g, C/25). Sohn et al. [29] prepared $Na_{0.7}MnO_2$ by a high-temperature solid-phase method and showed that this compound exhibits an initial discharge capacity of 176.4 mAh/g.

At present, not much is known about the performance of α-$NaMnO_2$ as a cathode material for Li-ion batteries. Therefore, we herein prepared monoclinic α-$NaMnO_2$ by a high-temperature solid-phase method and explored its electrochemical performance as a cathode material of a hybrid Li/Na-ion battery with a Li sheet as a counter electrode and a Li salt electrolyte, achieving a high first-cycle discharge capacity at a current density of 12.2 mA/g and a voltage of 2–4 V vs. Li/Li^+.

2. EXPERIMENTAL

2.1 Sample preparation

All reagents used in the experiment were pure and were used as received.

A 1.1:1 (mol/mol) mixture of Na_2CO_3 and in-house-prepared Mn_2O_3 was wetted by the addition of absolute ethyl alcohol, ball-milled for 6 h at 400 rpm, oven-dried at 80 °C for 12 h, pressed

into a pellet, and then heated in air at 750, 800, or 850 °C for 12 h or at 800 °C for 10, 12, or 14 h. After calcination, samples were immediately transferred into an Ar-filled glove box (MB10 Shanghai) to avoid contact with atmospheric moisture.

2.2 Sample characterization

The phase composition of calcined α-$NaMnO_2$ was probed by X-ray diffraction (XRD, Bruker D2) analysis, which was performed using Cu K_α radiation (30 kV, 10 mA) for 2θ = 10–70° at a scan rate of 0.02°/s. Sample microstructure was probed by transmission electron microscopy (TEM; Jeol JEM-2010FEF) and scanning electron microscopy (SEM; Hitachi SU8220), while elemental composition was determined by inductively coupled plasma-atomic emission spectroscopy (ICP-AES; ICPE-9000, Shimadzu).

2.3 Cell fabrication and electrochemical testing

As-synthesized α-$NaMnO_2$ was used to fabricate a coin cell battery that was subjected to electrochemical performance testing. Specifically, Al foil was coated with a slurry of 70 wt% active material, 20 wt% conductive agent (acetylene black), and 10 wt% binder (polyvinylidene fluoride) in *N*-methylpyrrolidone and dried in a vacuum oven at 110 °C for 12 h. After drying, the foil was cut into disks of ~10-mm diameter, and the assembly of CR-2025 button batteries was completed in the Ar-filled glove box. The electrolyte comprised a 1 M solution of $LiPF_6$ in ethylene carbonate:dimethyl carbonate:ethyl methyl carbonate (1:1:1, v/v/v). A polyethylene membrane (Celgard America) was used as a separator, and Li metal was used as the counter electrode.

Charge/discharge and cycle lifetime tests were performed using a LAND test system (CT2001A Wuhan) at room temperature and a current density of 12.2 mA/g over a voltage range of 2–4 V. Cyclic voltammetry (CV) and alternating-current (AC) impedance tests were performed using an electrochemical workstation (CHI650D Shanghai Chenhua) within a voltage range of 2–4 V and at a sweep rate of 0.1 mV/s. In addition, the above workstation was employed for AC impedance analysis, which was performed in a frequency range of 0.01 Hz to 0.1 MHz at an amplitude of 5 mV.

3. RESULTS AND DISCUSSION

3.1 Structural characterization

Figures 1a and b show the XRD patterns of α-$NaMnO_2$ sintered in air under different conditions, revealing that the main peaks could be ascribed to standard $NaMnO_2$ (JCPDS #25-0845), except for the peak located at 2θ = 15.8°, which was ascribed to $Na_{0.7}MnO_2$ (JCPDS #27-0752).

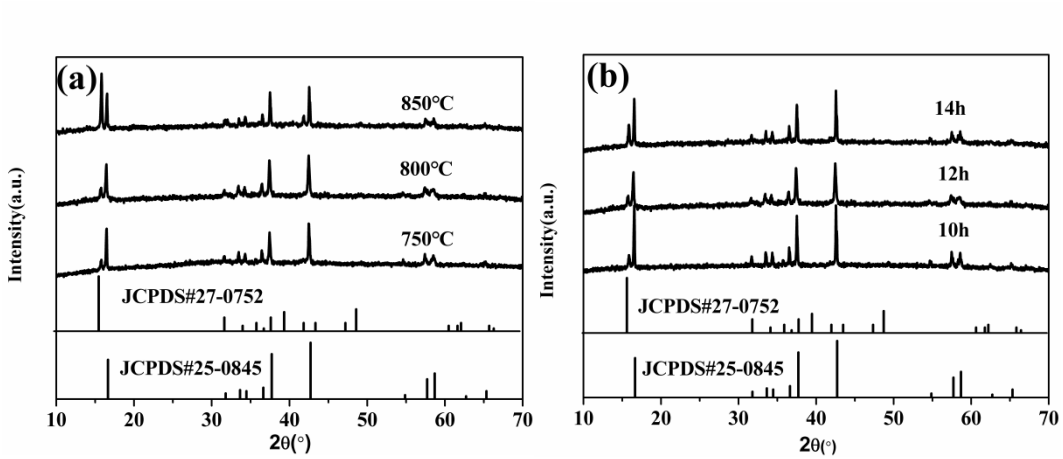

Figure 1. (a)XRD patterns of the α-$NaMnO_2$ samples prepared at 750, 800 and 850 °C for 12h.(b) XRD patterns of the α-$NaMnO_2$ samples prepared at 800 °C for 10, 12 and14h.

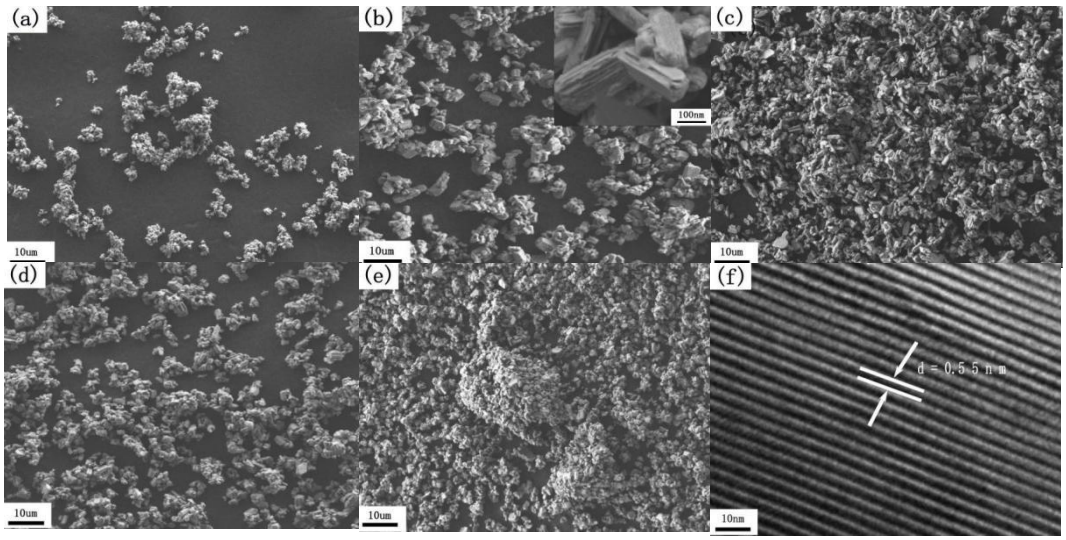

Figure 2. SEM images of α-$NaMnO_2$ synthesized at (a)750 °C for 12h (b) 800 °C for 12h (c) 850 °C for 12h (d) 800 °C for 10h (e)800 °C for 14h and (f) TEM image of the α-$NaMnO_2$ sample synthesized at 800 °C for 12h.

Figures 2a–c display SEM images of samples synthesized by 12-h annealing at 750–850 °C, while Figs. 2d–e show SEM images of samples synthesized by annealing at 800 °C for different times. Notably, specimens prepared using an annealing temperature of 750 °C or an annealing time of 10 h exhibited a low degree of crystallinity, while samples prepared using an annealing temperature of 850 °C or an annealing time of 14 h contained large particles, which was detrimental to material properties. The sample obtained by 12-h annealing at 800 °C exhibited good crystallinity and comprised small layered particles approximately 100 nm in size. Figure 2f presents representative TEM images of as-fabricated α-$NaMnO_2$, allowing the lattice spacing to be determined as 0.55 nm, which corresponded to the (001) plane and was in agreement with XRD results. Sample stoichiometric composition was determined by ICP-AES as Na:Mn = 0.94:1 (mol/mol).

3.2 Electrochemical performance

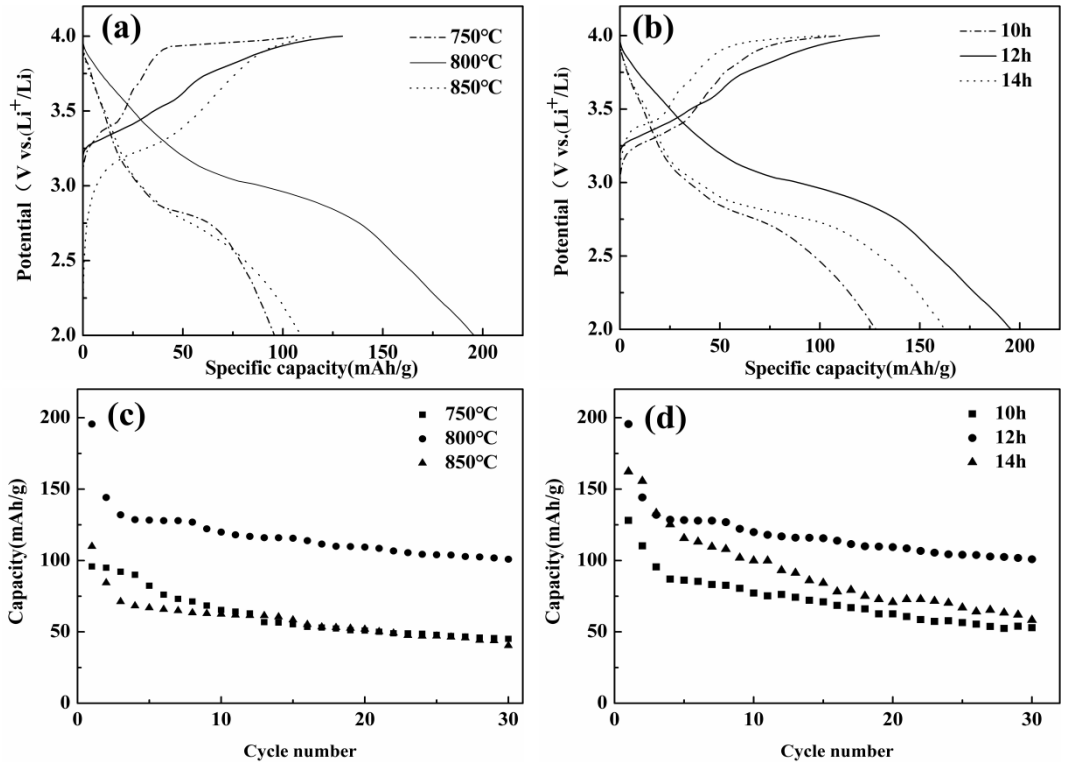

Figure 3. (a,c) Initial charge/discharge curves and cycling performances of the α-$NaMnO_2$ samples prepared at 750, 800 and 850 °C for 12h.(b,d)Initial charge/discharge curves and cycling performances of the α-NaMnO2 samples prepared at 800 °C for 10,12,14h.

Table 1. Comparison of electrochemical performance of Na_xMnO_2 materials (this paper and previous reported data).

Author	Material	Initial discharge capacity(mAh/g)	current density
Caballero et al.[29]	$Na_{0.6}MnO_2$	140	0.1 mA/cm^2
Ruffo et al. [18]	$Na_{0.44}MnO_2$	110	11mA/g
Sohn et al. [30]	$Na_{0.7}MnO_2$	176.4	20mA/g
Sample of this work	α-$NaMnO_2$	195.6	12.2mA/g

The electrochemical properties of α-$NaMnO_2$ specimens were determined by half-cell testing at room temperature. Figure 3a presents the initial charge/discharge curves of α-$NaMnO_2$ prepared by variable-temperature 12-h sintering that were recorded at a current density of 12.2 mA/g and voltages of 2–4 V, demonstrating that initial discharge capacities of 95.8, 195.6, and 128.1 mAh/g were obtained for sintering temperatures of 750, 800 and 850 °C, respectively. Figure 3b presents the first-cycle charge/discharge curves of samples calcined at 800 °C for different times, showing that discharge capacities of 109.9, 195.6, and 162.3 mAh/g were obtained for times of 10, 12, and 14h, respectively. Figure 3c and d present the cycling stabilities of different samples at a current density of 12.2 mA/g

and voltages of 2–4 V. In particular, Figure 3c shows the effect of sintering temperature at constant sintering time (12 h), revealing that discharge capacities of 45.2, 100.9, and 43.1 mAh/g were obtained after 30 cycles for samples calcined at 750, 800 and 850 °C, respectively. Figure 3d presents the effect of sintering time at constant sintering temperature, showing that discharge capacities of 52.9, 100.9, and 58.3 mAh/g were obtained after 30 cycles for samples calcined at 800 °C for 10, 12, and 14 h, respectively. In addition, the latter figures also demonstrate the presence of a charge/discharge plateau at 2.9–3.4 V. The discharge capacity first increased and then decreased with increasing calcination temperature and time, since low temperatures and short times prevented crystal growth, whereas high temperatures and long times promoted crystal agglomeration. Therefore, optimal electrochemical performance was observed for 12-h calcination at 800 °C.

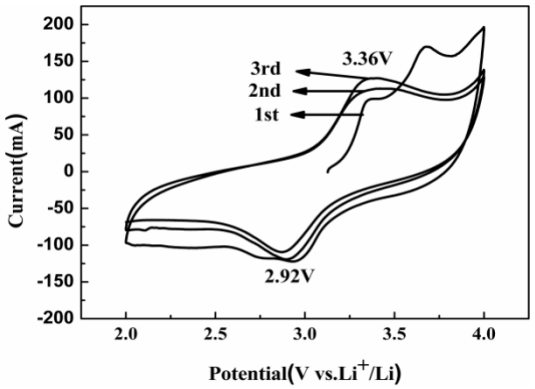

Figure 4. CV of α-$NaMnO_2$ samples prepared at 800 °C for 12h.

Figure 4 shows the first three CV curves of 800 °C/12 h α-$NaMnO_2$ recorded at a scan rate of 0.1 mV/s between 2 and 4 V, demonstrating the presence of a pair of redox peaks corresponding to the charge/discharge plateaus of voltage curves. Specifically, the oxidation peak was observed at ~3.36 V, while the reduction peak was located at ~2.92 V. The above CV curves did not completely overlap, indicating that the prepared samples featured poor cycling reversibility [30,31]. Thus, the electrochemical reversibility of α-$NaMnO_2$ was concluded to require further improvement, since this parameter has a crucial effect on cycling performance.

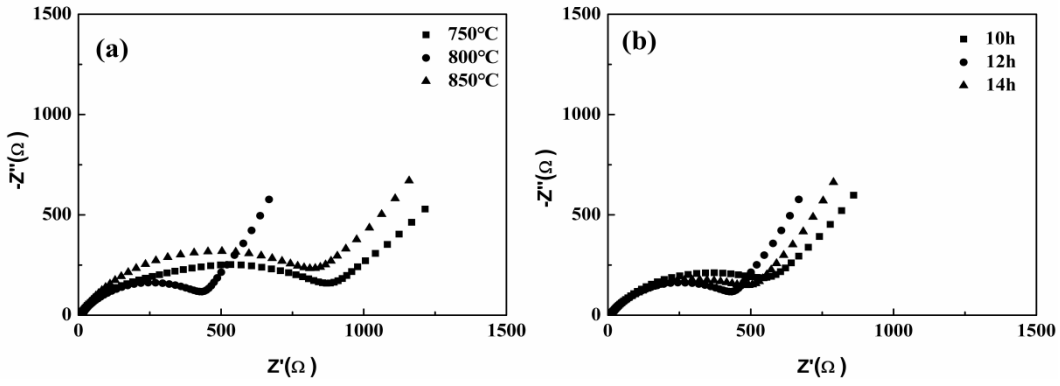

Figure 5. (a) EIS curves of α-$NaMnO_2$ samples prepared at 750, 800 and 850 °C for 12h.(b) EIS curves of α-$NaMnO_2$ samples prepared at 850 °C for 10,12 and 14h.

The electrochemical impedance (EIS) spectrum of the optimal sample (Fig. 5) was composed of several segments, featuring a line intersecting the real axis, a semicircle in the high-frequency region, and a straight line in the low-frequency region. The above semicircle represented electrochemical reaction impedance (R_{ct}), a parameter indicating the difficulty of charge transfer in a given electrochemical process. A line with a 45° slope in the low-frequency region represented the Warburg impedance, which indicates the ease of Li^+/Na^+ diffusion in the electrode [32,34]. Based on the presented information, the optimal sample featured a low charge transfer impedance of ~480 Ω and hence, superior electrochemical performance.

4. CONCLUSIONS

Monoclinic α-$NaMnO_2$ was successfully prepared by a conventional high-temperature solid-phase method and characterized by several instrumental techniques. The discharge capacity of α-$NaMnO_2$ first increased and then decreased with increasing calcination temperature and time, and the best electrochemical performance was observed for the sample calcined at 800 °C for 12 h. This optimal sample exhibited a high initial discharge capacity of 196.5 mAh/g, which, however, decreased to 101.9 mAh/g after 30 cycles. Compared to previously reported Na_xMnO_2 compounds, the optimal-performance specimen prepared herein features a higher first cycle discharge capacity, although its cycling stability still requires improvement.

ACKNOWLEDGMENTS
The study was supported by the National Natural Science Foundation of China (No. 21661030) and Xinjiang University Scientific Research Project(XJEDU2017S08)

References

1. S. Giri, D. Ghosh, A. Malas, C.K. Das, *J. Electron. Mater.*, 42 (2013) 2595.
2. J. Liu, J.G. Zhang, Z. Yang, J.P. Lemmon, C. Imhoff, G.L. Graff, L. Li, J. Hu, *Adv. Funct. Mater.*, 23 (2013) 929.
3. M. Armand, J.M. Tarascon, *Nat.*, 451 (2008) 652.
4. Z. Hou, X. Li, J. Liang, Y. zhu, Y. Qian, *J. Mater. Chem. A*, 3 (2014) 1400.
5. M.D. Slater, D. Kim, E. Lee, C.S. Johnson, *Adv. Funct. Mater.*, 23 (2013) 947.
6. M. Guignard, C. Didier, J. Darriet, P. Bordet, E. Elkaïm, C. Delmas, *Nat. Mater.*, 12 (2013) 74.
7. M.D. Slater, D.T. Kim, E. Lee, C.S. Johnson, *Adv. Funct. Mater.* 23 (2013) 947.
8. X. Ma, H. Chen, G. Ceder, *J. Electrochem. Soc.*, 158 (2011) A1307.
9. H. Yoshida, N. Yabuuchi, S. Komaba, *Electrochem. Commun.*, 34 (2013) 60.
10. W. Tang, X. Song, Y. Du, C. Peng, M. Lin, S. Xi, B. Tian, J. Zheng, Y. Wu, F. Pan, and K. P. Loh, *J. Mater. Chem. A,* 4 (2016) 4882.
11. T. Boyadzhieva, V. Koleva, R. Stoyanova , *PCCP*, 19 (2017).
12. Y.U. Park, J. Bai, L. Wang, G. yoon, W. Zhang, H. Kim, S Lee, S.W. Kim, J.P. Looney, K. Kang, F. Wang, *J. Am. Chem. Soc.*, 139 (2017) 12504.
13. Y. Zheng, P Zhang, S.Q. Wu, Y.H. Wen, Z.Z. Zhu, Y. Yang, *J. Electrochem. Soc.*, 160 (2013) A927.
14. D. Kundu, E. Talaie, V. Duffort, L.F. Nazar, *Cheminform*, 46 (2015) 3431.

15. S. Komaba, C. Takei, T. Nakayama, A. Ogata, N. Yabuuchi, *Electrochem. Commun.*, 12 (2010) 355.
16. M. D'Arienzo, R. Ruffo, R. Scotti, F. Morazzoni, C.M. Mari, S. Polizzi, *Phys. Chem. Chem. Phys.*, 14 (2012) 5945.
17. F. Sauvage , L. Laffont , J.M. Tarascon, E. Baudrin, *Inorg. Chem.*, 46 (2007) 3289.
18. R. Ruffo, R. Fathi, J.K. Dong, H.J. Young, M.M. Claudio, D.K. Kim, *Electrochim. Acta,* 108 (2013) 575.
19. E. Hosono, T. Saito, J. Hoshino, M. Okubo, Y. Saito, D. Nishio-Hamane, T. Kudo, H. Zhou, *J. Power Sources,* 217 (2012) 43.
20. J. Song, J. Gim, S. Kim, J. Kang, V. Mathew, D. Ahn, J. Kim, *Chem. - Asian J.*, 9 (2014) 1550.
21. A. Caballero, J. Morales, Aranda M.A.G. Aranda, *J. Mater. Chem.*, 12 (2002) 1142.
22. D.Su, C. Wang, H.J. Ahn, G. Wang, *Chem. - Eur. J.*, 19 (2013) 10884.
23. N. Bucher, S. Hartung, A. Nagasubramanian, *ACS Appl. Mater. Interfaces*, 6 (2014) 8059.
24. A.M. Abakumov, A.A. Tsirlin, I. Bakaimi, G.V. Tendeloo, *Chem. Mater.*, 26 (2014) 3306.
25. C. Liu, J. Li, P. Zhao, W. Guo, X. Yang, *J. Nanopart. Res.*, 17 (2015) 1.
26. Y. Li, Y. Wu, *Nano Res.*, 2 (2009) 54.
27. Y. Cao, L. Xiao, W. Wang, D. Choi, Z. Nie, J. Yu, L.V. Saraf, Z. Yang, J. Liu, *J. Adv. Mater.*, 23 (2011) 3155.
28. C. Delmas, C. Fouassier , P. Hagenmuller, *Physica B+C (Amsterdam)*, 99 (2007) 81.
29. D.R. Sohn, S.J. Lim, D.H. Nam, K.S. Hong, T.H. Kim, S.K. Oh, J.Y. Eom, *Electron. Mater. Lett.*, 14 (2017) 1.
30. P. Gao, L.Wang, L. Chen, X. Jiang, J. Pinto, G. Yang, *Electrochim. Acta*, 100 (2013) 125.
31. H. Li, Y. Li , L. Chen, H. Jiang, J. Wei, H. Wang, Y. Wang, *J. Alloys Compd.*, 617 (2014) 154.
32. Y.Q. Qiao, X.L. Wang, J.Y. Xiang, *Electrochim. Acta*, 56 (2011) 2269.
33. Z. Yang, J. Hu, Z. Chen, N. Zhang, *Rsc Advances*, 5 (2015) 17924.
34. J. Yan, W. Yuan, H. Xie, *Mater. Lett.*, 71 (2012) 1.